Spatial Distribution of Sensible and Latent Heat Flux in the URBANFLUXES case study city Basel (Switzerland)

Christian Feigenwinter[1], Eberhard Parlow[1], Roland Vogt[1], Michael Schmutz[1], Nektarios Chrysoulakis[2], Fredrik Lindberg[3], Mattia Marconcini[4], Fabio del Frate[5]

[1]Meteorology, Climatology, Remote Sensing, University of Basel, Switzerland
christian.feigenwinter@unibas.ch
[2]Foundation for Research and Technology – Hellas (FORTH), Heraklion, Crete, Greece
[3]Dept. of Earth Sciences, University of Gothenburg, Sweden
[4]German Remote Sensing Data Center: Land Surface, German Aerospace Center (DLR), Oberpfaffenhofen, Germany
[5]GEO-K s.r.l., Rome, Italy

***Abstract*—Turbulent sensible and latent heat fluxes are calculated by a combined method using micro-meteorological approaches (the Aerodynamic Resistance Method ARM), Earth Observation (EO) data and GIS-Techniques. The spatial distributions of turbulent heat fluxes were analyzed for 22 for the city of Basel (Switzerland), covering all seasons and different meteorological conditions. Seasonal variations in heat fluxes are strongly dependent on meteorological conditions, i.e. air temperature, water vapor saturation deficit and wind speed. The agreement of measured fluxes (by the Eddy Covariance method) with modeled fluxes in the weighted source area of the flux towers is moderate due to known drawbacks in the modelling approach and uncertainties inherent to EC measurements, particularly also in urban areas.**

Keywords— Urban Energy Balance, Eddy Covariance, Earth Observation, Aerodynamic Resistance Method, GIS, URBANFLUXES

I. INTRODUCTION

The URBANFLUXES Horizon 2020 project (urbanfluxes.eu) aims to derive the anthropogenic heat flux from Earth Observation (EO) data. Each component of the energy balance (net radiation R_n, sensible (Q_H) and latent (Q_E) heat flux, and storage heat flux ΔQ_S) is evaluated in a separate work package [1]. This study concentrates on the fluxes of sensible and latent heat. These fluxes are strongly modified by the properties of the urban surface, i.e. 3D geometry, high roughness, impervious surfaces, complex source/sink distribution and injections of heat and water into the urban atmosphere by human activities (traffic, heating, waste management, etc.). The spatial variability of urban terrain complicates their estimation. The existence of various surface types and different exposures to solar radiation in a complex surface geometry lead to significant variations in heat fluxes over short distances. This problem is well known, but for practical purposes, various simplifications that assume homogeneous properties at the surface like Monin–Obukhov Similarity Theory (MOST) [2] are still widely used to estimate the sensible heat flux in meso-scale models. Although MOST was originally derived for flat and homogeneous terrain, it is also applied over heterogeneous terrain, including cities [2].

II. METHODS

A. Flux calculation

The Aerodynamic Resistance Method (ARM) to estimate Q_H uses the simple relation (e.g. [3])

$$Q_H = \rho c_p \frac{T_s - T_a}{r_a} \tag{1}$$

where ρ is the density of air, c_p the specific heat of air at constant pressure, T_s is the surface temperature derived from satellite thermal infrared observations, T_a is the air temperature, and r_a is the aerodynamic resistance. Analogously, Q_E is expressed as

$$Q_E = \frac{\rho c_p}{\gamma} \frac{e_s^* - e_a}{r_a + r_s} \tag{2}$$

where e_s* is the saturation water vapor pressure at T_a, e_a is the atmospheric water vapor pressure, γ is the psychrometric constant and r_s is the stomatal resistance. Stomatal resistance is calculated after [4] using the simplified equation from [5]

$$\frac{1}{r_s} = \frac{f_1(T_a) f_2(PAR)}{r_{sMIN}} + \frac{1}{r_{cuticle}} \tag{3}$$

where PAR is the photosynthetic active radiation, r_{sMIN} is the minimum stomatal resistance and $r_{cuticle}$ is the canopy resistance related to the diffusion through the cuticle layer of leaves. Functions $f1$ and $f2$ are calculated as per [5]. Q_E is calculated by land cover type (fig. 1) and weighted by its fraction with the respective r_{sMIN} in every pixel. Values for r_{sMIN} used in this study are 500, 100, 70 and 50 s m^{-1} for bare soil, low vegetation, evergreen and deciduous, respectively.

The aerodynamic resistance r_a for sensible heat in (1) can be written as

978-1-5090-5808-2/17/$31.00 ©2017 IEEE

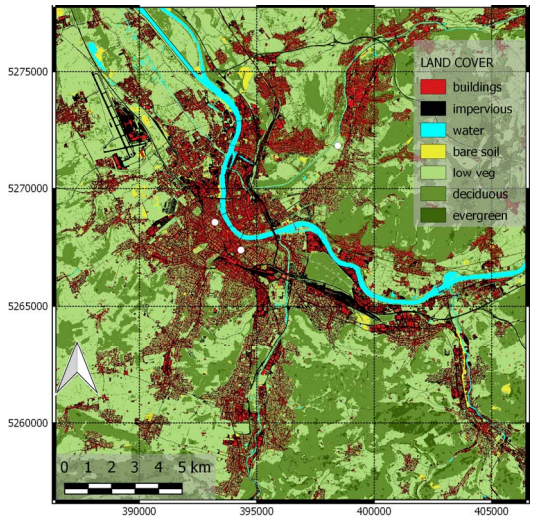

Fig. 1. Land cover map of Basel with flux towers (white points).

$$r_a = \frac{1}{u_* k}\left[ln\left(\frac{z_{ref}-z_d}{z_{0m}}\right) - \psi_h\left(\frac{z_{ref}-z_d}{L}\right) + \ln\left(\frac{z_{0m}}{z_{0h}}\right)\right] \quad (4)$$

and

$$u_* = Uk\left[ln\left(\frac{z_{ref}-z_d}{z_{0m}}\right) - \psi_m\left(\frac{z_{ref}-z_d}{L}\right) - \psi_m\left(\frac{z_{0m}}{L}\right)\right]^{-1} \quad (5)$$

where u_* is the friction velocity, k is the von Kármán constant (0.4), z_{ref} refers to the reference height, z_d is the zero-plane displacement height, L is the Monin-Obukhov length, z_{0m} is the roughness length for momentum, z_{0h} the roughness length for heat (accounting for the excess resistance when using radiometric surface temperatures [6]) and $\psi_{m,h}$ are the stability functions for momentum and heat, respectively [3]. Equation (5) can be used to estimate u_* from wind velocity U by iteration, if no direct measurements of the friction velocity are available [8]. z_{0h} values are usually reported as the dimensionless number $k\beta^{-1}$, defined as

$$k\beta^{-1} = ln\left(\frac{z_{0m}}{z_{0h}}\right) \quad (6)$$

and z_{0h} can be calculated after [3] by

$$z_{0h} = z_{0m}\left(7.4\exp(-\alpha Re^{0.25})\right) \quad (7)$$

where Re is the roughness Reynolds number and α is a parameter that varies with surface. Re is calculated by $Re = z_{0m} u_* / \nu$ with a kinematic molecular viscosity ν of 1.461×10^{-5} $m^2\ s^{-1}$.

Input for the calculation of roughness parameters, i.e. the morphometry, is derived from a digital surface model, in high spatial resolution (5 m) using the Urban Multi-scale Environmental Predictor (UMEP) [9]. UMEP output provides statistiscs of building heights and morphological parameters plane area index and frontal area index aggregated to the grid size (here 100 m). Roughness parameters z_{0m} and z_d are calculated by the real urban surfaces parameterization of [10].

B. Evaluation

The results are evaluated by the analysis of the calculated fluxes in the footprint [11] of the flux towers. Fluxes are measured by the Eddy Covariance method and processed with standard methods [12, 13]. Satellite derived surface temperatures are compared to the surface temperature T_{rad} calculated from the emitted longwave radiation in the radiation footprint [14] of the flux towers. T_{rad} is calculated by

$$T_{rad} = \left[\frac{L\uparrow-(1-\varepsilon)L\downarrow}{\sigma\varepsilon}\right]^{0.25} \quad (8)$$

where $L\uparrow,\downarrow$ is the upwelling and downwelling longwave radiation, respectively, ε is the emissivity of the surface (0.97) and σ is the Stefan Boltzmann constant. 50% of the radiometer signal origins from an area below the sensor with a radius equal to the height of the sensor [14]. For practical purposes, an area of 3 x 3 cells with the flux tower in the center was selected for the evaluation of T_S. The center cell was weighted 20 % and the adjacent cells 10 % each for the evaluation of T_s.

III. Study Area and Datasets

Here we present results from the URBANFLUXES case study city Basel (city population 200k, Basel agglomeration population 500k), a typical mid-sized mid-european city right at the border triangle France-Switzerland-Germany. Land Cover types (fig. 1) were derived from SPOT 5 data, land cover fractions were aggregated to the URBANFLUXES standard 100 m grid. Surface temperatures were calculated from Landsat 8 TIRS. Urban morphology parameters used for the calculation of atmospheric resistances in (4) are available from UMEP. For the parameter α in (7) we used a value of -0.8 for built-up areas as proposed for the city of Basel by [15] and the standard value of -2.46 from [3] for areas with low roughness, mainly the low vegetation land cover class, e.g. agricultural land use and bare soil.

Q_H and Q_E were calculated for 22 Landsat 8 scenes between FEB 2013 and DEC 2015 for Basel (overpass time around 11:15 UTC+1, fig. 3). Measured T_a was extrapolated to the full area using the dry adiabatic lapse rate of 0.0098 K m^{-1} to consider the topography ranging from 240 m to 800 m a.s.l.

Friction velocity u_* was extrapolated to the 100 m grid by iteration [8] using the measurements from the BKLI flux tower (fig. 4) as a starting value and roughness parameters z_{0m} and z_d. Note that measurements in the same season may vary considerably between different years with consequences for the modelled fluxes as shown in the overview in fig. 3.

IV. Results

A. Fluxes

Modeled Q_H and Q_E for the study area are shown in fig. 2 for the Landsat 8 overpass from 30 AUG 2015 at 1116 CET. Q_H shows highest values in the industrial areas, at the airport (NW of city center) and railway stations (areas with impervious land cover in fig. 1), in the inhabited areas in the city and in the densely populated valleys of the urban

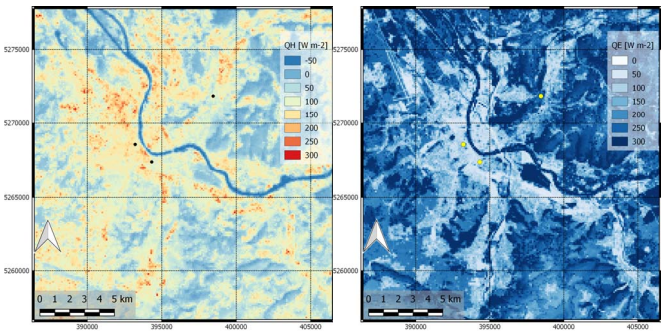

Fig. 2. Modeled sensible heat flux (left) and latent heat flux (right) for Basel during Landsat 8 overpass on 30 AUG 2015. Black and yellow points mark flux towers BKLI, BAES and BLER (from left to right).

agglomeration. Negative values are calculated for River Rhine, because the surface temperature of water bodies is lower (25 °C) than the surrounding air temperature (29 °C). Dense forests also show low sensible heat flux, because the foliage temperature is close to air temperature

. Largest latent heat fluxes Q_E origin from water bodies and dense forests. Urban parks and areas with low building density also show considerable amounts of evapotranspiration (up to 200 W m^{-2}). Note that T_a on this day was very high for the season (29° C) causing a high saturation deficit which again leads to high Q_E.

Though the most important input to Q_H in the ARM method is the difference between surface temperature and air temperature, the correlation is not always straightforward, as can be seen by the comparison of the scenes in fig.3. The general seasonal trend with highest fluxes for both, Q_H and Q_E (not shown), during the summer months is obvious, but interannual differences can be large.

B. Evaluation

Modeled Q_H and Q_E from the 22 Landsat scenes are evaluated by comparison with the measured fluxes in the weighted source area of the three Basel flux towers (fig. 4). The comparison of measured to modeled fluxes and tower T_{rad} to T_s are shown in figs. 5 and 6. Agreement between measured and modeled fluxes is generally poor though the flux maps in figs. 2 and 3 show reasonable values. Modeled fluxes in the footprint of the flux towers do mostly underestimate the measured fluxes and the scatter is large. Relative underestimation of Q_E is larger than for Q_H but evaporative fluxes are of course lower in urban areas than in the rural surroundings. Possible reasons leading to this results are discussed in section V. Regression statistics (not shown) for T_s are better than for the heat fluxes, nevertheless, differences may reach up to 4 K (fig. 6). Satellite derived T_s are higher at the urban flux towers BKLI and BAES and lower at the rural/suburban flux tower BLER. We address this to the different fields of view, i.e., the radiation sensor mounted on an urban flux tower "sees" a considerable amount of walls, which are more influenced by shadow effects and may lead to

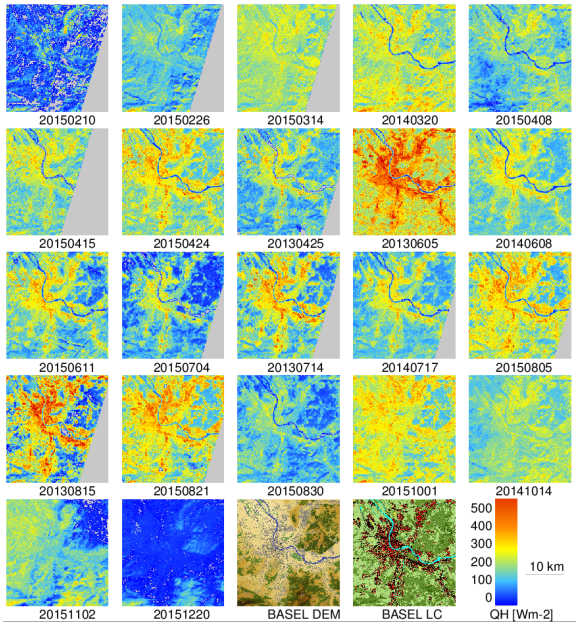

Fig. 3. Sensible heat flux for 22 scenes for Basel case study (sorted by season from upper left (FEB) to lower right (DEC). Lower row additionally shows digital elevation model (DEM) and Land Cover map (LC).

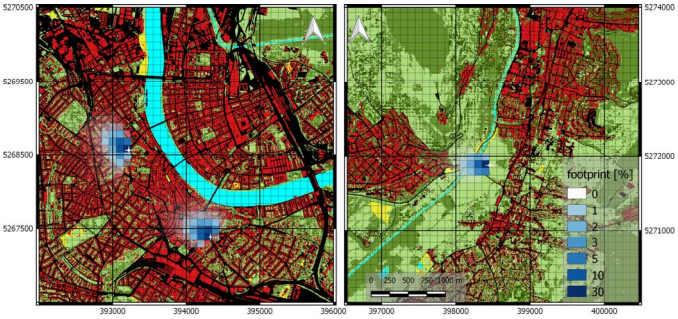

Fig. 4. Weighted footprints for 30 AUG 2015 satellite overpass (11:00 UTC+1). Left: Urban flux towers BKLI and BAES. Right: Rural/suburban flux tower BLER. Reference system is UTM 32N.

cooler T_{rad}. Additional uncertainty is introduced by the use of a bulk emissivity for EO derived T_s and atmospheric correction.

V. Discussion and Outlook

The analysis of modeled Q_H and Q_E from 22 Landsat scenes for the URBANFLUXES case study city Basel shows reasonable results, but the validation with in-situ measurements is generally moderate. Possible reasons for the observed deviations are:

- The uncertainty inherent to EC measurements may range from 10% for Q_H to up to 25 % for trace gases (e.g. [16]). Representativeness of flux tower measurements in urban environments is reduced due to the heterogeneity of urban neighbourhoods [12]. Large (inherent) variations in EC measurements between averaging intervals additionally increase this uncertainty.
- Known drawbacks of the ARM method: input parameters (T_a, wv) have to be spatially derived from in-situ

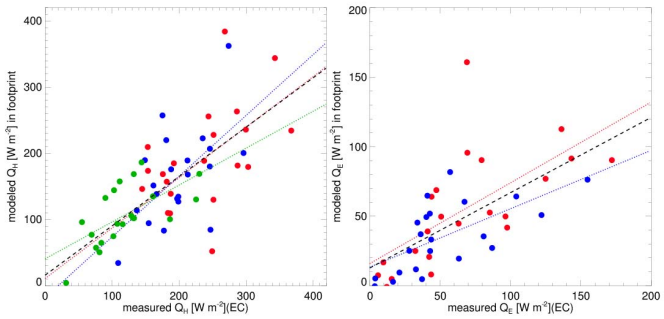

Fig. 5. Comparison of modeled (y-axis) and measured (x-axis) Q_H (left) and Q_E (right) for flux towers BKLI (red), BAES (blue) and BLER (green) with regression lines.

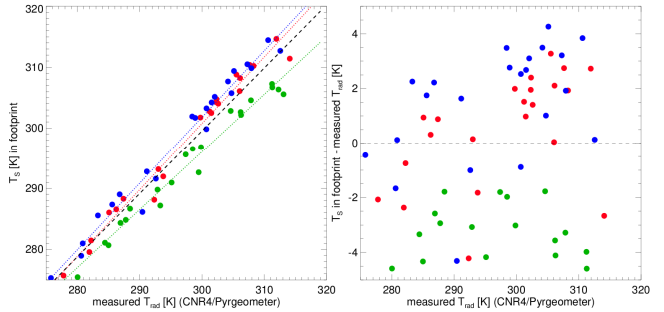

Fig. 6. Left: As fig. 5 but for surface temperature T_{rad} (x-axis) against satellite derived surface temperature T_s (y-axis) Right: Same as left panel, but for the differences $T_s - T_{rad}$

measurements and may differ from "true" values in certain areas; further large uncertainties exist in the calculation of the aerodynamic resistance including $k\beta^{-1}$.

- Uncertainties in the calculation of flux tower source areas used for comparison with modelled fluxes [17].
- Difficulties to measure evapotranspiration in general and in urban areas in part.

Finally, modelled fluxes may be improved by examination of uncertainties in T_s related to emissivity, thermal anisotropy and atmospheric correction in urban areas.

As URBANFLUXES will model all terms of the urban energy balance independently to derive the anthropogenic heat flux, the next step within this project is to combine the presented results with EO derived storage term ΔQ_S and net radiation R_n and then analyze the energy balance closure.

ACKNOWLEDGMENT

The project leading to this application has received funding from the European Union's Horizon 2020 research and innovation program under grant agreement No 637519 (URBANFLUXES).

REFERENCES

[1] N. Chrysoulakis et al., "Urban Energy Budget Estimation from Sentinels: The URBANFLUXES Project," Mapping Urban Areas from Space, Frascati, Italy, 4-5 November 2015

[2] T. Foken, "50 Years of the Monin–Obukhov Similarity Theory", *Boundary Layer Meteorol.,* vol. 119, pp. 431-447, 2006.

[3] W. Brutsaert, "Evaporation into the atmosphere," D. Reidel Publ. Co. Boston. 1982

[4] S. Kato, Y. Yamaguchi, C.C. Liu, C.Y. Sun, "Surface heat balance analysis of Tainan City on March 6, 2001 using ASTER and Formosat-2 data," *sensors*, vol. 8, pp. 6026 – 6044, 2008.

[5] K. Nishida, R.R. Nemani, S.W. Running, J.M. Glassy, "An operational remote sensing algorithm of land surface evaporation,", *J. Geo. Res*, vol. 108, doi: 10.1029/2002JD002062

[6] J.A.Voogt, C.S.B. Grimmond, "Modeling surface sensible heat flux using surface radiative temperatures in a simple urban area," *J. Appl. Meteorol.*, vol. 39, pp. 1679-1699, 2000.

[7] U. Högström, "Non-dimensional wind and temperature profiles in the atmospheric surface layer: A re-evaluation," *Topics in Micrometeorology*. A Festschrift for Arch Dyer. Springer Netherlands, pp.55-78, 1988

[8] C.S.B. Grimmond and H.A. Cleugh, "A simple method to determine Obukhov Lengths for suburban areas," *J. Appl. Meteorol.,* vol. 33, pp. 435-440, 1994.

[9] F. Lindberg, C.S.B. Grimmond, S. Onomura, L. Järvi, "UMEP - An integrated tool for urban climatology and climate-sensitive planning applications", International Conference on Urban Climatology (ICUC9), Toulouse, France, 2015.

[10] M. Kanda, A. Inagaki, T. Miyamoto, M. Gryschka, S. Raasch, "A new aerodynamic parametrization for real urban surfaces," *Boundary- Layer Meteorol.*, vol. 148, pp. 357-377, 2013

[11] R. Kormann, F.X. Meixner, "An analytical footprint model for non-neutral stratification," *Boundary-Layer Meteorol.,* vol 99, pp. 207-224, 2001.

[12] C. Feigenwinter, R. Vogt, A. Christen, "Eddy Covariance Measurements Over Urban Areas," pp. 377–397, in: Eddy Covariance A Practical Guide to Measurement and Data Analysis. Heidelberg, New York, Springer Atmospheric Sciences, p. 430. Springer. 2012

[13] X. Lee, W. Massman, B. Law (eds.), "Handbook of Micrometeorology", Heidelberg, New York, Springer, 2005.

[14] W.E. Reifsnyder, "Radiation geometry in the measurement and interpretation of radiation balance," *Agr. Meteorol.*, vol. 4, pp. 255-265, 1967.

[15] C.M. Frey and E. Parlow, "Determination of the aerodynamic resistance to heat using morphometric methods," *EARSel eProceedings* vol. 9:2, pp. 52-63, 2010.

[16] A.D. Richardson et al., "Uncertainty Quantification," pp. 173–207, in: Eddy Covariance - a Practical Guide to Measurement and Data Analysis. Heidelberg, New York, Springer Atmospheric Sciences, p. 430. Springer. 2012

[17] A. Hellsten et al., "Footprint evaluation for flux and concentration measurements for an urban-like canopy with coupled Lagrangian stochastic and LES simulation models," *Bound.-Layer Meteorol.,* vol. 157.2, pp.157- 191, 2015